

# Visualization of moiré magnons in monolayer ferromagnet

Somesh Chandra Ganguli,<sup>1,\*</sup> Markus Aapro,<sup>1</sup> Shawulienu Kezilebieke,<sup>2</sup>  
Mohammad Amini,<sup>1</sup> Jose L. Lado,<sup>1,\*</sup> and Peter Liljeroth<sup>1,\*</sup>

<sup>1</sup>*Department of Applied Physics, Aalto University, FI-00076 Aalto, Finland*

<sup>2</sup>*Department of Physics, Department of Chemistry and Nanoscience Center,  
University of Jyväskylä, FI-40014 University of Jyväskylä, Finland*

(Dated: January 24, 2023)

Two-dimensional magnetic materials provide an ideal platform to explore collective many-body excitations associated with spin fluctuations. In particular, it should be feasible to explore, manipulate and ultimately design magnonic excitations in two-dimensional van der Waals magnets in a controllable way. Here we demonstrate the emergence of moiré magnon excitations, stemming from the interplay of spin-excitations in monolayer CrBr<sub>3</sub> and the moiré pattern arising from the lattice mismatch with the underlying substrate. The existence of moiré magnons is further confirmed via inelastic quasiparticle interference, showing the appearance of a dispersion pattern correlated with the moiré length scale. Our results provide a direct visualization in real-space of the dispersion of moiré magnons, demonstrating the versatility of moiré patterns in creating emerging many-body excitations.

The recent discovery of two dimensional van der Waals (vdW) monolayer magnetic materials has opened new avenues for scalable, defect-free samples for spintronic applications and artificial designer materials [1–10]. It provides an exciting opportunity to control and manipulate magnetism in two-dimensions [11–14], and create new emergent states in vdW heterostructures [15–19]. A common feature of two-dimensional materials is the appearance of moiré patterns due to the lattice mismatch or twist between the monolayer and the substrate. Using the twist degree of freedom has emerged as a powerful strategy to design new quantum states [20–23]. Paradigmatic examples are the emergent correlated and topological states in graphene moiré multilayers [24, 25], ferroelectricity in hexagonal boron nitride moiré bilayers [26], moiré excitons in twisted MoSe<sub>2</sub>/WSe<sub>2</sub> [27], and moiré magnetism in CrI<sub>3</sub> moiré bilayers [28]. The emergence of moiré phenomena in magnetic van der Waals materials is a newly explored field, and in particular the possibility of creating magnon moiré excitations remains an open problem in twistrionics.

Chromium trihalides (CrX<sub>3</sub>, X= Cl, Br and I, Fig. 1a) have been established as a prominent family of 2D magnetic materials [29] with all three showing ferromagnetic order, where the easy axis is out-of-plane for CrBr<sub>3</sub> [6, 7] and CrI<sub>3</sub> [2], and in-plane for CrCl<sub>3</sub> [30]. We have carried out low-temperature scanning tunneling microscopy (STM) and spectroscopy (STS) to probe the magnon excitations in monolayer CrBr<sub>3</sub>. We show that the results can be understood in terms of moiré magnons arising from a reconstruction of the magnon dispersion by the moiré pattern formed by the lattice mismatch between CrBr<sub>3</sub> and the substrate. This leads to new van Hove singularities in the magnon spectral function that are correlated with the moiré length scale. Furthermore, by exploiting quasiparticle interference with inelastic spectroscopy, we directly probe the magnon dispersion in

reciprocal space, allowing us to map the moiré magnon spectra. Our results demonstrate the emergence of moiré magnons and the impact of moiré patterns on the magnetic excitations of 2D materials.

We have carried out experiments on CrBr<sub>3</sub> monolayers on a highly-oriented pyrolytic graphite (HOPG) substrate at a  $T = 350$  mK (see Methods section for more experimental details). Typical STM topography image (Fig. 1b) shows both bright triangular protrusions arising from the bromine atoms in the CrBr<sub>3</sub> layer as well as a longer length-scale variation corresponding to the moiré pattern, which arises from the lattice mismatch between the CrBr<sub>3</sub> monolayer and the HOPG substrate. Magnetic excitations can be probed via inelastic tunneling spectroscopy (IETS) and they should result in bias-symmetric steps in the  $dI/dV$  signal [6, 31–33]. We observe clear inelastic excitations experimentally as demonstrated in Fig. 1c that shows both the measured  $dI/dV$  (symmetrized) and numerically differentiated and smoothed  $d^2I/dV^2$  signals (see Supplementary Information (SI) for details). As schematically illustrated in Fig. 1d, for a ferromagnetic system, we would expect the  $dI/dV$  to correspond to the integrated magnon DOS while the  $d^2I/dV^2$  signal directly corresponds to the local magnon spectral function. It is immediately obvious that our experimental  $d^2I/dV^2$  contains many more peaks than expected for a typical magnon spectrum. We explain this discrepancy below as arising from the moiré-induced modification of the magnon spectrum.

The physics behind the moiré magnons can be understood starting from the anisotropic Heisenberg Hamiltonian [34, 35] describing the spin excitations in a magnetic two-dimensional system (see SI for details)

$$\mathcal{H} = - \sum_{ij} J_{ij} \vec{S}_i \cdot \vec{S}_j - \sum_{ij} K_{ij} S_i^z S_j^z + \mathcal{H}_V \quad (1)$$

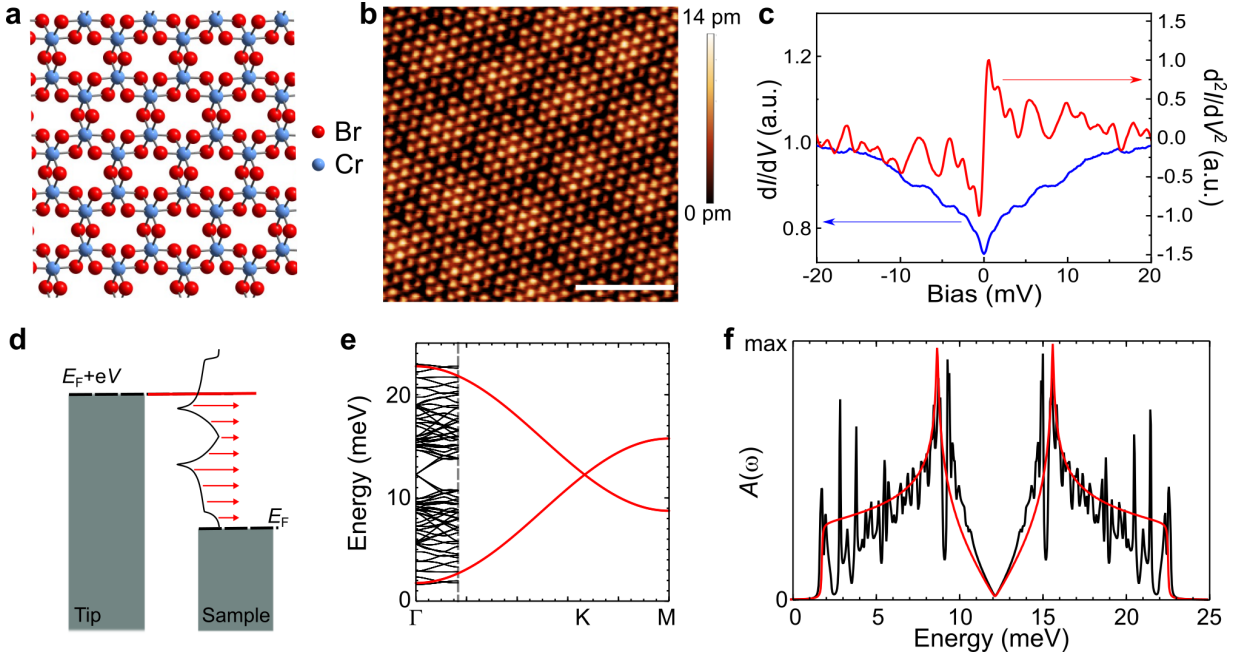


FIG. 1. **Probing moiré magnons in CrBr<sub>3</sub> with IETS.** **a**, Schematic of the CrBr<sub>3</sub> structure. **b**, Atomically resolved image of CrBr<sub>3</sub> on HOPG. Image was taken at sample bias 1.5 V. Scale bar 5 nm. **c**, Averaged and symmetrized  $dI/dV$  (blue) and numerically differentiated  $d^2I/dV^2$  (red) obtained in monolayer CrBr<sub>3</sub> on HOPG. **d**, Schematic of inelastic tunneling spectroscopy of magnons. **e**, Unfolded magnon bands and moiré-folded magnon mini-bands. **f**, Unfolded (red) and moiré-folded (black) magnonic spectral functions.

with  $J_{ij}$  the spatially modulated isotropic exchange coupling,  $K_{ij}$  the anisotropic exchange and  $S_n^\alpha$  the local  $S = 3/2$  operators in the Cr atoms, [36] forming a honeycomb lattice (Figs. 1a). The term  $\mathcal{H}_V$  contains other potential terms in the Hamiltonian including Dzyaloshinskii-Moriya interaction, biquadratic exchange, single-ion anisotropy and Kitaev interaction, which for the sake of simplicity are not included in the next discussion as their role is not important for the emergence of moiré magnons. The local moments at the Cr-sites have a ferromagnetic coupling via superexchange through Br atom, parametrized by  $J_{ij}$ . The existence of the substrate leads to an additional exchange interaction mediated by the RKKY interaction. This substrate-mediated RKKY interaction depends on the local stacking between CrBr<sub>3</sub> and HOPG, which in turn is controlled by the moiré between HOPG and CrBr<sub>3</sub>. This modulation in real space leads to the change of the exchange constants  $J_{ij}$  [7, 28, 37, 38] and, in turn, the spin stiffness through the moiré unit cell [39–42]. Moreover, potential small structural distortions lead to a modulation of the superexchange interaction, both of which follow the same periodicity as the moiré pattern. Holstein-Primakoff mapping [43] allows the magnonic Hamiltonian to be written in terms of the bosonic magnon operators

$$\mathcal{H} = - \sum_{ij} \gamma_{ij} a_i^\dagger a_j + \sum_n \Delta_n a_n^\dagger a_n + \text{h.c.} \quad (2)$$

with  $\gamma_{ij} \sim J_{ij}$  controlling the spin stiffness and  $\langle \Delta_n \rangle$  determines the magnon gap, and  $a_n^\dagger, a_n$  are the creation and annihilation magnon operators. For CrBr<sub>3</sub>, first principles calculations [44] predict a bandwidth of the magnon spectra of  $\sim 30$  meV in the absence of a moiré pattern, and in the following we take that the moiré modulations changes the local exchange while keeping the global bandwidth approximately equal to the uniform case.

In the absence of the moiré pattern, the magnon dispersion features two magnon bands stemming from the two Cr atoms in the unit cell. The magnon dispersion shows Dirac points when neglecting small contributions coming from  $\mathcal{H}_V$ , and a low energy quadratic dispersion with a gap controlled by  $K$ . In the presence of the moiré pattern, the real-space modulation of  $\gamma_{ij}$  leads to the appearance of magnon mini-bands in the moiré supercell, as shown in Fig. 1e. The multiple folding of the original moiré bands and induced anticrossings driven by the moiré exchange modulation gives rise to a whole new set of moiré singularities, as shown in Fig. 1f.

We have carried out inelastic tunneling spectroscopy experiments (parameters mentioned in the Methods section) over a range of CrBr<sub>3</sub> islands with different moiré periodicities allowing us to address the impact of the underlying moiré pattern on the magnetic excitations. Figs. 2a,c show the effect of the different moiré length scales (moiré wavelengths of 7 and 3.6 nm) on the inelastic excitations. The anti-symmetrised  $d^2I/dV^2$  (details

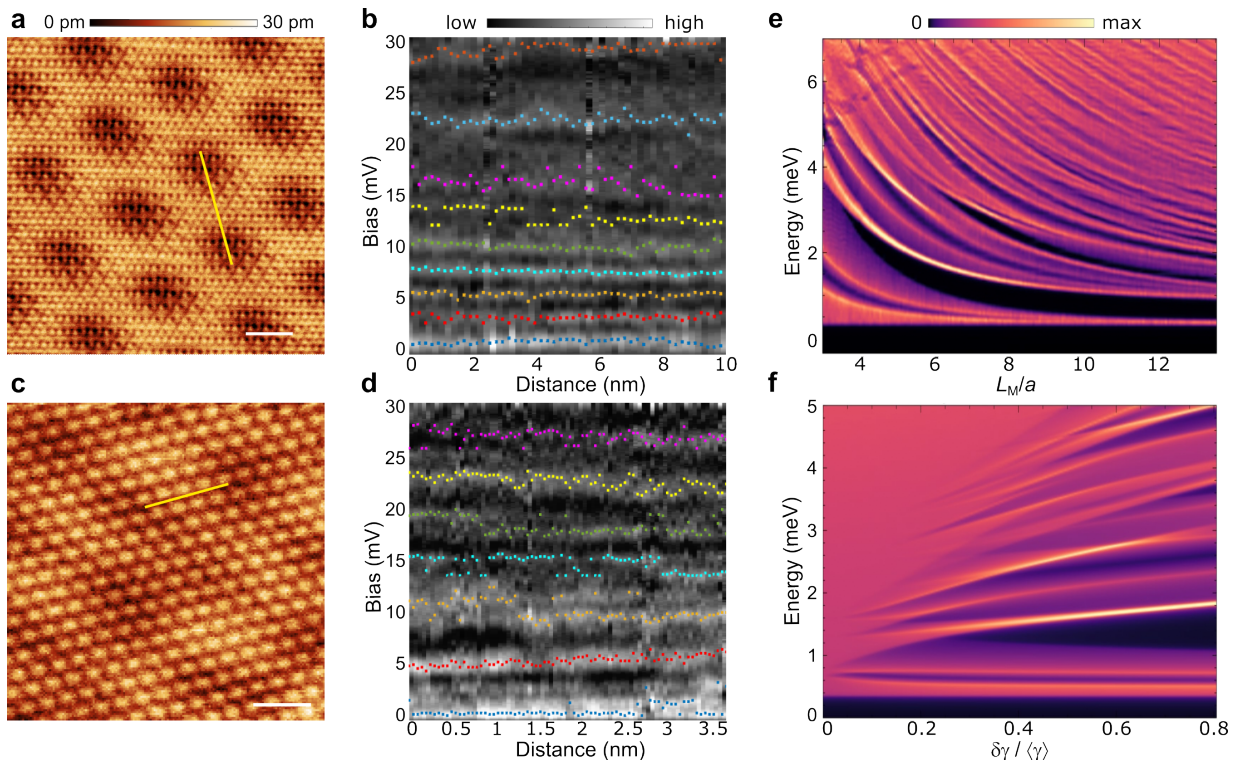


FIG. 2. **Moiré magnons in CrBr<sub>3</sub>.** **a,b**, Area with moiré wavelength 7 nm (Scale bar 4 nm. Image bias 1 V), spatial dependence of antisymmetrised  $d^2I/dV^2$  (b) with spectra taken along yellow line in panel (a). **c,d** Area with moiré wavelength 3.6 nm (Scale bar 2 nm. Image bias 2 V), spatial dependence of antisymmetrised  $d^2I/dV^2$  (d) with spectra taken along yellow line in panel (c). In (b),(d), colored points indicate the locations of maxima in the  $d^2I/dV^2$  corresponding to the van Hove singularities in the magnon spectral function (see SI). **e,f** Theoretical dependence of the magnon spectral function with the moiré length (e) and with the strength of the exchange modulation (f).

in the SI) shows strong peaks that are spatially quite uniform as shown in Fig. 2b,d. The moiré magnon features are expected to be the most visible at the bottom of the magnon band due to the folding into the moiré Brillouin zone (see Fig. 1f). In addition, the higher energy inelastic excitations are less intense in the experimental spectra, which can be understood through magnon-magnon interaction effects [45]. Therefore, we focus on the lower energy features and comparing Figs. 2c,d, it is clear that there are more inelastic features with a smaller energy spacing in the experiments on the larger length-scale moiré pattern (see SI for the statistics of inelastic peak energies).

The dependence of low energy inelastic magnon peaks with the moiré wavelengths can be rationalized from the reconstruction of the magnon bands triggered by the moiré pattern. The momentum folding of the magnon structure depends on the length of the moiré pattern, leading to magnon van Hove singularities whose energy location depends on the specific moiré. In particular, longer moiré lengths give rise to magnon van Hove singularities with a smaller energy spacing, as observed experimentally. This phenomenology is captured with the moiré Heisenberg model, as shown in Fig. 2e. The relative intensity of the moiré van Hove singularities is con-

trolled by the strength of the moiré modulation as shown in Fig. 2f, highlighting that the observation of moiré magnons can allow inferring the value of the real space modulation of the exchange constants.

While our experiments are consistent with the expectation that the observed inelastic features correspond to magnetic excitations, they could also correspond to inelastic excitations of phonons. However, earlier experiments on tunneling devices have shown that the modes with sufficient electron-phonon coupling are at higher energies (above 25 meV) [46] than the features we observe in our experiments. Additionally, the magnetic origin of the excitations is usually probed by carrying out experiments under an external magnetic field. We have done these experiments (see SI for the results); however, the HOPG substrate shows very clear and strong signatures of Landau levels at high magnetic fields that completely overwhelm the signal from the magnetic excitations in the CrBr<sub>3</sub> layer. It is also not possible to subtract the signal from the Landau levels as the Landau level spectra of bare HOPG and HOPG covered by CrBr<sub>3</sub> are different arising from the sensitivity of the Landau levels to the local potential [47]. At low-magnetic fields (< 0.5 T), the signal due to the magnetic excitations is clearly visible,



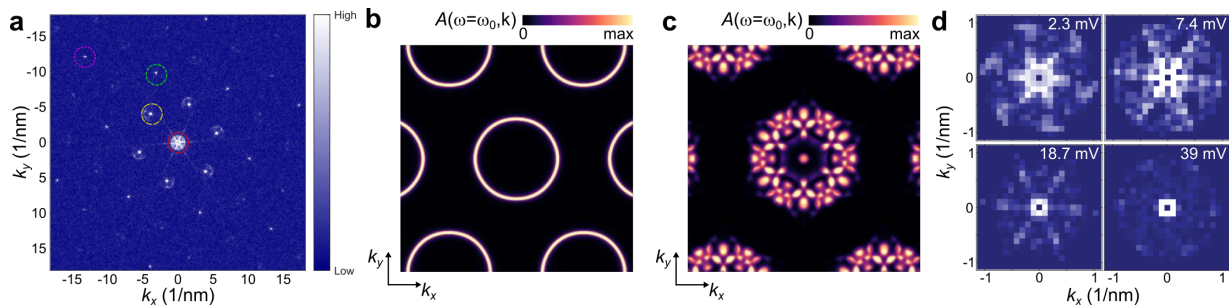


FIG. 3. **Quasiparticle interference of magnons.** **a**, FFT of a constant-current  $dI/dV$  map at a bias voltage of 7.4 mV. Red, yellow, green and magenta dotted circles indicate real space lengthscales of 7 nm, 1.25 nm, 6 Å, 4 Å, respectively. **b,c**, Calculated momentum-resolved spectral function of magnon  $A(\omega, \mathbf{k})$  at constant energy of 5 meV in the absence (b) and presence of the moiré pattern (c). **d**, Zoomed-in FFTs of the experimental  $dI/dV$  signal around the  $\Gamma$ -point at the bias voltages indicated in the panels.

but the shifts due to the Zeeman energy are too small to be reliably detected.

The presence of moiré magnons can be demonstrated even more convincingly through inelastic quasiparticle interference spectroscopy that allows a direct visualization of the length scale of the moiré magnons. We note that this technique has been used to demonstrate the emergence of quantum spin liquid signatures in monolayer 1T-TaSe<sub>2</sub> [48]. The differential conductance  $dI/dV$  is proportional to the total number of magnons that can be excited with that energy. In the presence of weak scattering, the total number of magnons will be spatially modulated. The dispersion of the moiré magnons can be directly probed by visualizing the Fourier transform of the spatially resolved  $dI/dV$ , shown in Fig. 3a, known as quasiparticle interference (QPI). The signature of moiré magnons is directly visible in the QPI due to the reconstruction of the magnon spectra. Specifically, the Fourier transform of the  $dI/dV$ , in the following denoted as  $\Xi(\omega, \mathbf{q})$  stems from inelastic magnon tunneling processes as  $\Xi(\omega, \mathbf{q}) \sim \int A(\omega, \mathbf{k})A(\omega, \mathbf{k} + \mathbf{q})d^2\mathbf{k}$ , where  $A(\omega, \mathbf{k})$  is the magnon spectral function. As a result, the magnon QPI reflects a self-convolution of the magnon dispersion, directly reflecting magnon reconstructions in reciprocal space.

While this kind of QPI features could also arise from elastic scattering between electronic states, it is very unlikely in the present case. First of all, CrBr<sub>3</sub> is an insulator and has no electronic states close to the Fermi level. We could of course still in principle observe QPI from the electronic states of the HOPG substrate; however, in that case one would expect QPI signal over a large bias range since HOPG has states at all energies. This is in contrast to our experimental results and hence, the QPI features most likely correspond to the magnon excitations.

To explore the dispersion of the magnonic bands, we performed constant current  $dI/dV$  maps at various energies (parameters mentioned in the Methods section). The typical FFT of the  $dI/dV$  maps has strong peaks

at characteristic reciprocal space points, indicating different topographic periodicities present. The green, magenta, red and yellow dotted circles in Fig. 3a represents Cr-Cr (6 Å), Br-Br (4 Å), moiré (7 nm) and possible  $\sqrt{3} \times \sqrt{3}$  Kekulé distortion (1.25 nm) length scales. The high-symmetry points, especially  $\Gamma$  and  $K$  points have features around them.

Theoretically, in the absence in the moiré pattern, the magnon spectral function at energies below 8 meV should feature a simple circular shape coming from the magnon dispersion  $\epsilon(\mathbf{k}) \sim |\mathbf{k}|^2$  as shown in Fig. 3b. This featureless circular shape leads to the well-known disc-like QPI, that does not show a complex angular structure. In stark contrast, in the presence of the moiré, the moiré modulation leads to a full new set features in the magnon dispersion as shown in Fig. 3c, as a direct consequence of the magnon moiré mini-bands. The inelastic contribution to the QPI gives rise to the different scattering events associated with the states in Fig. 3c, directly reflecting the emergent dispersion of the moiré bands. In particular, the moiré magnon generating QPI will give rise to very short wavelength features appearing around  $\Gamma$  point in the QPI.

These theoretical moiré QPI predictions can be directly compared with our experimental data (Fig. 2c). In order to factor out the impact of the topographic moiré modulation in the QPI, we first remove the peaks associated with the moiré length, whose origin is purely structural. Around the  $\Gamma$  point, after removing the intensity due to the moiré, we see an internal interference pattern strongly dependent on the energy and ultimately vanishing above  $\sim 25$  mV (Fig. 3d). It must be noted that, in the absence of a moiré pattern, no strong energy dependence of the QPI is expected around the  $\Gamma$  point. In stark contrast, the presence of moiré magnons leads to an energy-dependent interference pattern around the  $\Gamma$  point in the full energy window due to the non-trivial interplay between the different magnon moiré bands. The previous phenomenology directly demonstrates the



emergence of quasiparticle interference associated with magnons, featuring fluctuations in the moiré length scale and spanning over the whole energy window in which magnons fluctuations appear in  $\text{CrBr}_3$ .

To summarize, we have demonstrated the emergence of moiré magnon excitations in 2D monolayer ferromagnet. By using inelastic spectroscopy, we showed that the existence of moiré patterns with different moiré lengths leads to different reconstructions of the moiré spectra. The existence of moiré magnons is further confirmed via inelastic quasiparticle interference, showing the appearance of a dispersion pattern correlated with the moiré length scale. Our results provide a direct visualization in real space of the dispersion of moiré magnons, demonstrating the versatility of moiré patterns in creating emergent many-body excitations.

## METHODS

**Sample growth:** The  $\text{CrBr}_3$  thin film was grown on freshly cleaved HOPG substrates by compound source molecular beam epitaxy. The anhydrous  $\text{CrBr}_3$  flakes of 99 % purity was evaporated by Knudsen cell. Before growth, the cells were degassed up to the growth temperature  $350^\circ\text{C}$  until the vacuum was better than  $1 \times 10^{-8}$  mbar. The growth rate was determined by checking the coverage of the as-grown samples by STM.

**STM measurements:** Subsequent to the growth, the sample was transferred to a low-temperature STM (Unisoku USM-1300) housed in the same UHV system. STM imaging and STS experiments were performed at  $T = 350$  mK. STM imaging was performed in constant current mode. Differential conductance ( $dI/dV$ ) spectra were measured using standard lock-in techniques sweeping the sample bias in an open feedback loop with a.c bias modulation at a frequency of 873.7 Hz. For the  $dI/dV$  maps in Fig. 2b,d, the amplitude of bias modulation was 500  $\mu\text{V}$  and the current set point was 500 pA. For constant current  $dI/dV$  maps in Fig. 3a,d, the amplitude of bias modulation was kept to 5% of the applied d.c. bias, and the current set point was 200 pA. The raw images were drift corrected by Lawler-Fujita algorithm [49] and symmetrized to increase the signal to noise ratio of the QPI signal (described in SI).

---

\* Email: somesh.ganguli@aalto.fi, jose.lado@aalto.fi, peter.liljeroth@aalto.fi

- [1] Cheng Gong, Lin Li, Zhenglu Li, Huiwen Ji, Alex Stern, Yang Xia, Ting Cao, Wei Bao, Chenzhe Wang, Yuan Wang, and et al., “Discovery of intrinsic ferromagnetism in two-dimensional van der Waals crystals,” *Nature* **546**, 265–269 (2017).
- [2] Bevin Huang, Genevieve Clark, Efrén Navarro-Moratalla, Dahlia R. Klein, Ran Cheng, Kyle L. Seyler, Ding Zhong, Emma Schmidgall, Michael A. McGuire, David H. Cobden, and et al., “Layer-dependent ferromagnetism in a van der Waals crystal down to the monolayer limit,” *Nature* **546**, 270–273 (2017).
- [3] Kenneth S. Burch, David Mandrus, and Je-Geun Park, “Magnetism in two-dimensional van der Waals materials,” *Nature* **563**, 47–52 (2018).
- [4] Lebing Chen, Jae-Ho Chung, Bin Gao, Tong Chen, Matthew B. Stone, Alexander I. Kolesnikov, Qingzhen Huang, and Pengcheng Dai, “Topological spin excitations in honeycomb ferromagnet  $\text{CrI}_3$ ,” *Phys. Rev. X* **8**, 041028 (2018).
- [5] Lebing Chen, Jae-Ho Chung, Matthew B. Stone, Alexander I. Kolesnikov, Barry Winn, V. Ovidiu Garlea, Douglas L. Abernathy, Bin Gao, Mathias Augustin, Elton J. G. Santos, and Pengcheng Dai, “Magnetic field effect on topological spin excitations in  $\text{CrI}_3$ ,” *Phys. Rev. X* **11**, 031047 (2021).
- [6] D. Ghazaryan, M. T. Greenaway, Z. Wang, V. H. Guarochico-Moreira, I. J. Vera-Marun, J. Yin, Y. Liao, S. V. Morozov, O. Kristanovski, A. I. Lichtenstein, and et al., “Magnon-assisted tunnelling in van der Waals heterostructures based on  $\text{CrBr}_3$ ,” *Nat. Electron.* **1**, 344–349 (2018).
- [7] Weijong Chen, Zeyuan Sun, Zhongjie Wang, Lehua Gu, Xiaodong Xu, Shiwei Wu, and Chunlei Gao, “Direct observation of van der Waals stacking-dependent interlayer magnetism,” *Science* **366**, 983–987 (2019).
- [8] Hyun Ho Kim, Bowen Yang, Siwen Li, Shengwei Jiang, Chenhao Jin, Zui Tao, George Nichols, Francois Sfigakis, Shazhou Zhong, Chenghe Li, and et al., “Evolution of interlayer and intralayer magnetism in three atomically thin chromium trihalides,” *Proc. Nat. Acad. Sci.* **116**, 11131–11136 (2019).
- [9] M. Blei, J. L. Lado, Q. Song, D. Dey, O. Erten, V. Pardo, R. Comin, S. Tongay, and A. S. Botana, “Synthesis, engineering, and theory of 2D van der Waals magnets,” *Appl. Phys. Rev.* **8**, 021301 (2021).
- [10] Asimpunya Mitra, Alberto Corticelli, Pedro Ribeiro, and Paul A. McClarty, “Magnon Interference Tunneling Spectroscopy as a Probe of 2D Magnetism,” arXiv e-prints, arXiv:2110.02662 (2021), [arXiv:2110.02662 \[cond-mat.mes-hall\]](https://arxiv.org/abs/2110.02662).
- [11] Shengwei Jiang, Lizhong Li, Zefang Wang, Kin Fai Mak, and Jie Shan, “Controlling magnetism in 2D  $\text{CrI}_3$  by electrostatic doping,” *Nat. Nanotech.* **13**, 549–553 (2018).
- [12] Bevin Huang, Genevieve Clark, Dahlia R. Klein, David MacNeill, Efrén Navarro-Moratalla, Kyle L. Seyler, Nathan Wilson, Michael A. McGuire, David H. Cobden, Di Xiao, and et al., “Electrical control of 2D magnetism in bilayer  $\text{CrI}_3$ ,” *Nat. Nanotechnol.* **13**, 544–548 (2018).
- [13] Zhi Wang, Tongyao Zhang, Mei Ding, Baojuan Dong, Yanxu Li, Maolin Chen, Xiaoxi Li, Jianqi Huang, Hanwen Wang, Xiaotian Zhao, and et al., “Electric-field control of magnetism in a few-layered van der Waals ferromagnetic semiconductor,” *Nat. Nanotechnol.* **13**, 554–559 (2018).
- [14] Tingxin Li, Shengwei Jiang, Nikhil Sivadas, Zefang Wang, Yang Xu, Daniel Weber, Joshua E. Goldberger, Kenji Watanabe, Takashi Taniguchi, Craig J. Fennie, and et al., “Pressure-controlled interlayer magnetism in atomically thin  $\text{CrI}_3$ ,” *Nat. Mater.* **18**, 1303–1308 (2019).
- [15] Ding Zhong, Kyle L. Seyler, Xiayu Linpeng, Ran Cheng,

- Nikhil Sivadas, Bevin Huang, Emma Schmidgall, Takashi Taniguchi, Kenji Watanabe, Michael A. McGuire, and et al., “Van der Waals engineering of ferromagnetic semiconductor heterostructures for spin and valleytronics,” *Sci. Adv.* **3**, e1603113 (2017).
- [16] Kyle L. Seyler, Ding Zhong, Bevin Huang, Xiayu Linpeng, Nathan P. Wilson, Takashi Taniguchi, Kenji Watanabe, Wang Yao, Di Xiao, Michael A. McGuire, and et al., “Valley manipulation by optically tuning the magnetic proximity effect in  $\text{WSe}_2/\text{CrI}_3$  heterostructures,” *Nano Lett.* **18**, 3823–3828 (2018).
- [17] Shawulien Kezilebieke, Md Nurul Huda, Viliam Vaño, Markus Aapro, Somesh C. Ganguli, Orlando J. Silveira, Szczepan Ghodzik, Adam S. Foster, Teemu Ojanen, and Peter Liljeroth, “Topological superconductivity in a van der Waals heterostructure,” *Nature* **588**, 424–428 (2020).
- [18] Shawulien Kezilebieke, Viliam Vaño, Md N. Huda, Markus Aapro, Somesh C. Ganguli, Peter Liljeroth, and Jose L. Lado, “Moiré-enabled topological superconductivity,” *Nano Lett.* **22**, 328–333 (2022).
- [19] Viliam Vaño, Mohammad Amini, Somesh Chandra Ganguli, Guangze Chen, Jose L. Lado, Shawulien Kezilebieke, and Peter Liljeroth, “Artificial heavy fermions in a van der Waals heterostructure,” *Nature* **599**, 582–586 (2021).
- [20] E. Suárez Morell, J. D. Correa, P. Vargas, M. Pacheco, and Z. Barticevic, “Flat bands in slightly twisted bilayer graphene: Tight-binding calculations,” *Phys. Rev. B* **82**, 121407(R) (2010).
- [21] J. M. B. Lopes dos Santos, N. M. R. Peres, and A. H. Castro Neto, “Graphene bilayer with a twist: Electronic structure,” *Phys. Rev. Lett.* **99**, 256802 (2007).
- [22] B. Hunt, J. D. Sanchez-Yamagishi, A. F. Young, M. Yankowitz, B. J. LeRoy, K. Watanabe, T. Taniguchi, P. Moon, M. Koshino, P. Jarillo-Herrero, and et al., “Massive Dirac fermions and Hofstadter butterfly in a van der Waals heterostructure,” *Science* **340**, 1427–1430 (2013).
- [23] Guohong Li, A. Luican, J. M. B. Lopes dos Santos, A. H. Castro Neto, A. Reina, J. Kong, and E. Y. Andrei, “Observation of van Hove singularities in twisted graphene layers,” *Nat. Phys.* **6**, 109–113 (2009).
- [24] Yuan Cao, Valla Fatemi, Shiang Fang, Kenji Watanabe, Takashi Taniguchi, Efthimios Kaxiras, and Pablo Jarillo-Herrero, “Unconventional superconductivity in magic-angle graphene superlattices,” *Nature* **556**, 43–50 (2018).
- [25] M. Serlin, C. L. Tschirhart, H. Polshyn, Y. Zhang, J. Zhu, K. Watanabe, T. Taniguchi, L. Balents, and A. F. Young, “Intrinsic quantized anomalous Hall effect in a moiré heterostructure,” *Science* **367**, 900–903 (2020).
- [26] Kenji Yasuda, Xirui Wang, Kenji Watanabe, Takashi Taniguchi, and Pablo Jarillo-Herrero, “Stacking-engineered ferroelectricity in bilayer boron nitride,” *Science* **372**, 1458–1462 (2021).
- [27] Kha Tran, Galan Moody, Fengcheng Wu, Xiaobo Lu, Junho Choi, Kyoungwan Kim, Amrithes Rai, Daniel A. Sanchez, Jiamin Quan, Akshay Singh, and et al., “Evidence for moiré excitons in van der Waals heterostructures,” *Nature* **567**, 71–75 (2019).
- [28] Tiancheng Song, Qi-Chao Sun, Eric Anderson, Chong Wang, Jimin Qian, Takashi Taniguchi, Kenji Watanabe, Michael A. McGuire, Rainer Stöhr, Di Xiao, Ting Cao, Jörg Wrachtrup, and Xiaodong Xu, “Direct visualization of magnetic domains and moiré magnetism in twisted 2D magnets,” *Science* **374**, 1140–1144 (2021).
- [29] Michael McGuire, “Crystal and magnetic structures in layered, transition metal dihalides and trihalides,” *Crytals* **7**, 121 (2017).
- [30] Amilcar Bedoya-Pinto, Jing-Rong Ji, Avinandra K. Pandeya, Pierluigi Gargiani, Manuel Valvidares, Paolo Sessi, James M. Taylor, Florin Radu, Kai Chang, and Stuart S. P. Parkin, “Intrinsic 2D-XY ferromagnetism in a van der Waals monolayer,” *Science* **374**, 616–620 (2021).
- [31] A. Spinelli, B. Bryant, F. Delgado, J. Fernández-Rossier, and A. F. Otte, “Imaging of spin waves in atomically designed nanomagnets,” *Nat. Mater.* **13**, 782–785 (2014).
- [32] Markus Ternes, “Spin excitations and correlations in scanning tunneling spectroscopy,” *New J. Phys.* **17**, 063016 (2015).
- [33] D. R. Klein, D. MacNeill, J. L. Lado, D. Soriano, E. Navarro-Moratalla, K. Watanabe, T. Taniguchi, S. Manni, P. Canfield, J. Fernández-Rossier, and P. Jarillo-Herrero, “Probing magnetism in 2D van der Waals crystalline insulators via electron tunneling,” *Science* **360**, 1218–1222 (2018).
- [34] J L Lado and J Fernández-Rossier, “On the origin of magnetic anisotropy in two dimensional  $\text{CrI}_3$ ,” *2D Materials* **4**, 035002 (2017).
- [35] M. Gibertini, M. Koperski, A. F. Morpurgo, and K. S. Novoselov, “Magnetic 2D materials and heterostructures,” *Nat. Nanotechnol.* **14**, 408–419 (2019).
- [36] We note that additional terms can be included in the Hamiltonian, leading to analogous results [4, 34, 35, 50].
- [37] Nikhil Sivadas, Satoshi Okamoto, Xiaodong Xu, Craig J. Fennie, and Di Xiao, “Stacking-dependent magnetism in bilayer  $\text{CrI}_3$ ,” *Nano Lett.* **18**, 7658–7664 (2018).
- [38] Yang Xu, Ariana Ray, Yu-Tsun Shao, Shengwei Jiang, Daniel Weber, Joshua E. Goldberger, Kenji Watanabe, Takashi Taniguchi, David A. Muller, Kin Fai Mak, and Jie Shan, “Emergence of a noncollinear magnetic state in twisted bilayer  $\text{CrI}_3$ ,” arXiv e-prints, arXiv:2103.09850 (2021), arXiv:2103.09850 [cond-mat.mtrl-sci].
- [39] Yu-Hang Li and Ran Cheng, “Moiré magnons in twisted bilayer magnets with collinear order,” *Phys. Rev. B* **102**, 094404 (2020).
- [40] Chong Wang, Yuan Gao, Hongyan Lv, Xiaodong Xu, and Di Xiao, “Stacking domain wall magnons in twisted van der Waals magnets,” *Phys. Rev. Lett.* **125**, 247201 (2020).
- [41] Kyoung-Min Kim, Do Hoon Kiem, Grigory Bednik, Myung Joon Han, and Moon Jip Park, “Theory of moire magnets and topological magnons: Applications to twisted bilayer  $\text{CrI}_3$ ,” arXiv e-prints, arXiv:2206.05264 (2022), arXiv:2206.05264 [cond-mat.str-el].
- [42] David Soriano, “Domain wall formation and magnon localization in twisted chromium trihalides,” *Phys. Status Solidi Rapid Res. Lett.* **16**, 2200078 (2022).
- [43] T. Holstein and H. Primakoff, “Field dependence of the intrinsic domain magnetization of a ferromagnet,” *Phys. Rev.* **58**, 1098–1113 (1940).
- [44] Wei-Bing Zhang, Qian Qu, Peng Zhu, and Chi-Hang Lam, “Robust intrinsic ferromagnetism and half semiconductivity in stable two-dimensional single-layer chromium trihalides,” *J. Mater. Chem. C* **3**, 12457–12468 (2015).
- [45] Sergey S. Pershoguba, Saikat Banerjee, J. C. Lashley, Jihwey Park, Hans Ågren, Gabriel Aeppli, and Alexan-

- der V. Balatsky, “Dirac magnons in honeycomb ferromagnets,” *Phys. Rev. X* **8**, 011010 (2018).
- [46] D. Ghazaryan, M. T. Greenaway, Z. Wang, V. H. Guarochico-Moreira, I. J. Vera-Marun, J. Yin, Y. Liao, S. V. Morozov, O. Kristanovski, A. I. Lichtenstein, M. I. Katsnelson, F. Withers, A. Mishchenko, L. Eaves, A. K. Geim, K. S. Novoselov, and A. Misra, “Magnon-assisted tunnelling in van der Waals heterostructures based on CrBr<sub>3</sub>,” *Nat. Electron.* **1**, 344–349 (2018).
- [47] D. Haude, M. Morgenstern, I. Meinel, and R. Wiesendanger, “Local density of states of a three-dimensional conductor in the extreme quantum limit,” *Phys. Rev. Lett.* **86**, 1582–1585 (2001).
- [48] Wei Ruan, Yi Chen, Shujie Tang, Jinwoong Hwang, Hsin-Zon Tsai, Ryan L. Lee, Meng Wu, Hyejin Ryu, Salman Kahn, Franklin Liou, and et al., “Evidence for quantum spin liquid behaviour in single-layer 1T-TaSe<sub>2</sub> from scanning tunnelling microscopy,” *Nat. Phys.* **17**, 1154–1161 (2021).
- [49] MJ Lawler, K Fujita, Jhinhwan Lee, AR Schmidt, Y Kohsaka, Chung Koo Kim, H Eisaki, S Uchida, JC Davis, JP Sethna, *et al.*, “Intra-unit-cell electronic nematicity of the high-T<sub>c</sub> copper-oxide pseudogap states,” *Nature* **466**, 347–351 (2010).
- [50] Thomas A. Tartaglia, Joseph N. Tang, Jose L. Lado, Faranak Bahrami, Mykola Abramchuk, Gregory T. Mc-

Candless, Meaghan C. Doyle, Kenneth S. Burch, Ying Ran, Julia Y. Chan, and Fazel Tafti, “Accessing new magnetic regimes by tuning the ligand spin-orbit coupling in van der Waals magnets,” *Sci. Adv.* **6**, eabb9379 (2020).

## ACKNOWLEDGMENTS

This research made use of the Aalto Nanomicroscopy Center (Aalto NMC) facilities and was supported by the European Research Council (ERC-2017-AdG no. 788185 “Artificial Designer Materials”) and Academy of Finland (Academy professor funding nos. 318995 and 320555, Academy research fellow no. 331342 and 336243), and the Jane and Aatos Erkko Foundation. We acknowledge the computational resources provided by the Aalto Science-IT project.

## COMPETING INTERESTS

The authors declare no competing interests.



# Supplementary Information: Visualization of moiré magnons in monolayer ferromagnet

Somesh Chandra Ganguli,<sup>1,\*</sup> Markus Aapro,<sup>1</sup> Shawulienu Kezilebieke,<sup>2</sup>  
 Mohammad Amini,<sup>1</sup> Jose L. Lado,<sup>1,\*</sup> and Peter Liljeroth<sup>1,\*</sup>

<sup>1</sup>*Department of Applied Physics, Aalto University, FI-00076 Aalto, Finland*

<sup>2</sup>*Department of Physics, Department of Chemistry and Nanoscience Center, University of Jyväskylä, FI-40014 University of Jyväskylä, Finland*

## S1. DETERMINING THE INELASTIC SPECTRAL FUNCTION

The experimental  $dI/dV$  signal (Fig. S1a) is numerically differentiated to obtain  $d^2I/dV^2$  (Fig. S1b). The numerical  $d^2I/dV^2$  is smoothed by Savitzky–Golay method to obtain smoothed  $d^2I/dV^2$  (Fig. S1c) and the antisymmetrised  $d^2I/dV^2$  is determined as  $(d^2I/dV^2(V) - d^2I/dV^2(-V))/2$ .

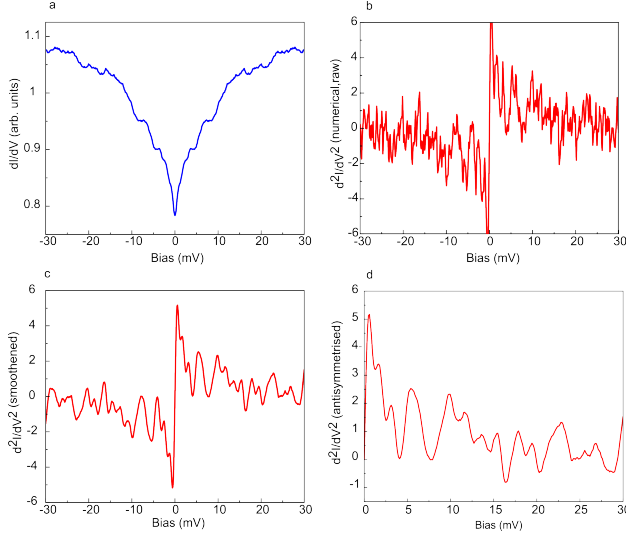


FIG. S1. Numerically determined inelastic spectral function: (a) Experimental  $dI/dV$ , (b) numerically differentiated  $d^2I/dV^2$ , (c) smoothed  $d^2I/dV^2$ , and (d) antisymmetrised  $d^2I/dV^2$ .

## S2. HISTOGRAM OF SPATIALLY DEPENDENT INELASTIC EXCITATIONS

We determined the energies of the inelastic peaks corresponding to the two different moiré areas in Figs. 2b, d. We observe that, specific number of inelastic peaks appear throughout albeit with some spatial variations in the same moiré area from the histogram plot of the energy values at different spatial locations (Fig. S2a,b). However, the number of inelastic peaks and their energies vary in two different moiré areas, with the larger moiré area having larger number of peaks (Fig. S2a,b).

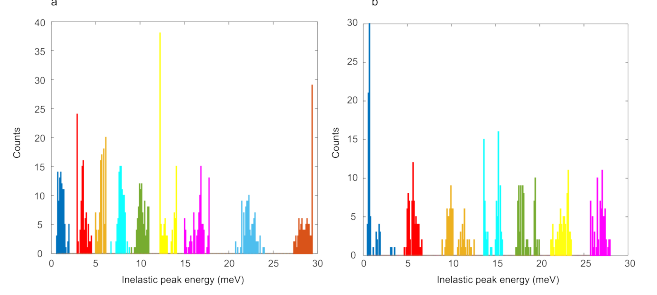


FIG. S2. Histogram of inelastic excitation energies corresponding to the (a) 7 nm moiré area, (b) 3.6 nm moiré area. The colors refer to individual miniband energies for the corresponding moiré areas in Figs. 2b, d.

## S3. MAGNETIC FIELD DEPENDENCE OF THE INELASTIC EXCITATIONS

When an external out-of-plane magnetic field is applied, the van Hove singularities in the magnonic band are expected to disperse linearly with the magnitude of the applied field. However, with increasing magnetic field, we observe a change of  $dI/dV$  signal from having step features to peak-like features (Fig. S3a, b, c). In the presence of an external magnetic field, the substrate HOPG shows strong peak-like features in  $dI/dV$  (Fig. S3d). They correspond to Landau levels (LL) due to quasi-two dimensional nature of conduction electrons within HOPG<sup>1,2</sup>. These strong signals in the  $dI/dV$  channel from the HOPG increases the number of peak like features observed in CrBr<sub>3</sub> and it makes it difficult to quantify the shifts of the magnetic excitations at high magnetic fields.

## S4. THEORETICAL MODEL

### A. Magnon Hamiltonian

Here we elaborate on the theoretical model accounting for magnetic excitations in CrBr<sub>3</sub>. The magnetic Cr sites realize a  $S = 3/2$  honeycomb lattice, with a Heisenberg

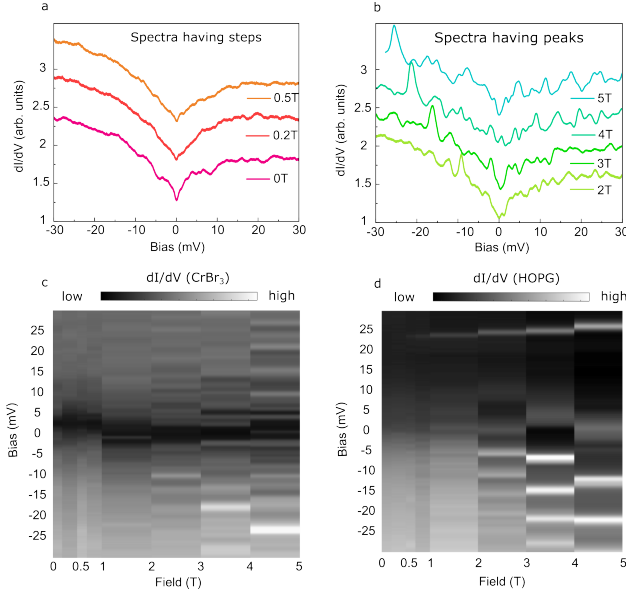


FIG. S3. (a, b) Magnetic field dependence of the differential conductance ( $dI/dV$ ) on  $\text{CrBr}_3$  showing step-like features in low magnetic fields (a) and peak-like features in high magnetic fields (b). (c) Full Magnetic field dependence of ( $dI/dV$ ) on  $\text{CrBr}_3$ . (d) Magnetic field dependence of the differential conductance ( $dI/dV$ ) on HOPG showing the appearance of Landau levels.

Hamiltonian of the form

$$\mathcal{H} = - \sum_{\langle ij \rangle} J_{ij} \vec{S}_i \cdot \vec{S}_j - K \sum_{\langle ij \rangle} S_i^z S_j^z - D \sum_i (S_i^z)^2 + \mathcal{H}_{HO} \quad (1)$$

where  $J_{ij}$  are the isotropic exchange coupling,  $K$  the anisotropic exchange,  $D$  the single ion anisotropic. From the fundamental point of view, the terms  $K$  and  $D$  give rise to a small gap in the magnon gap, whereas  $J_{ij}$  gives rise to the magnon moiré bands. The term  $\mathcal{H}_{HO}$  includes additional terms to the Hamiltonian including Kitaev exchange<sup>3</sup>, biquadratic exchange<sup>4</sup>, Dzyaloshinskii-Moriya interaction<sup>5</sup>, and dipolar coupling<sup>6</sup>. For the sake of concreteness, we will focus our discussion on the modulation of the exchange coupling  $J_{ij} = J((\mathbf{r}_i + \mathbf{r}_j)/2)$ , which is expected to be the strongest modulation<sup>7-10</sup>.

We take as starting point the ferromagnetic state of the Hamiltonian Eq. 1. We derive the magnonic Hamiltonian using a Holstein-Primakoff transformation<sup>11</sup> in the low temperature regime as  $S_n^z = S - a_n^\dagger a_n$ ,  $S_n^- \approx \sqrt{2S} a_n^\dagger$  and  $S_n^+ \approx \sqrt{2S} a_n$ , with  $a_n^\dagger$   $a_n$  creation and annihilation magnon operators in site  $n$ . The bosonic magnonic Hamiltonian takes the form

$$\mathcal{H} = - \sum_{ij} \gamma_{ij} a_i^\dagger a_j + \Delta \sum_i a_i^\dagger a_i + \text{h.c.} \quad (2)$$

where  $\gamma_{ij} \sim J_{ij}$  and  $\Delta$  controls the magnon gap, leading to a gapless spectra for  $D = K = 0$ . As a reference, the

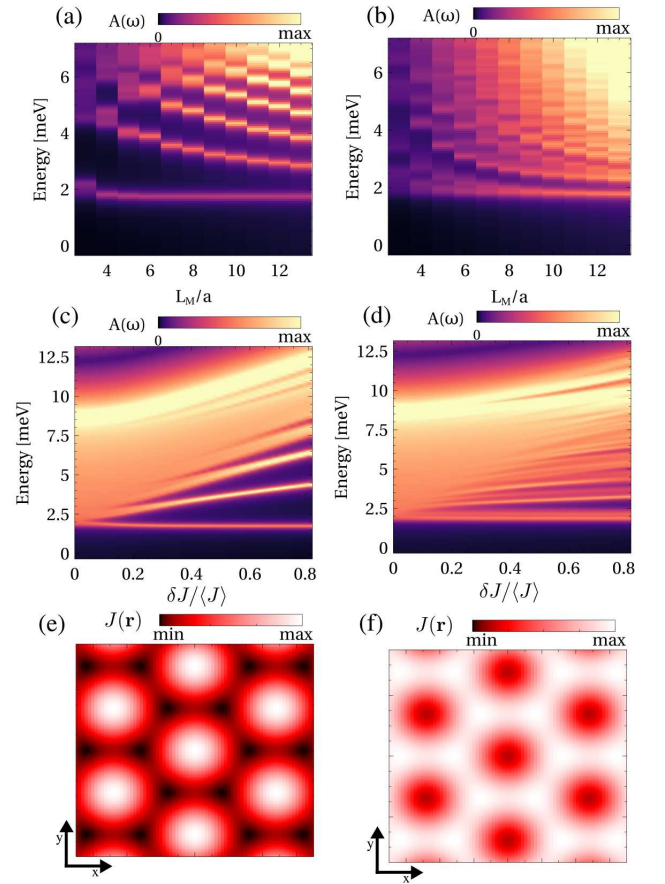


FIG. S4. (a,b) Magnon spectral function as a function of the strength of the moiré potential and (b,c) as a function of the moiré length. Panels (a,c) and (b,d) correspond to different exchange modulations, as shown in panels (e,f), respectively.

full magnon spectra of  $\text{CrBr}_3$  is approximately 25 meV<sup>12</sup>, consistent with first principles calculations results<sup>13</sup>.

## B. Moiré magnons

The existence of a moiré pattern leads to a modulation of the exchange constants  $J_{ij}$ , in turn leading to a modulation of the magnon hoppings  $\gamma_{ij}$ . From the structural point of view, the spatially dependent stacking leads to a modulation of the super-exchange interaction mediated by the substrate. We show in Fig. S4 the evolution of the magnon spectral function as a function of the moiré length  $L_M$  of the modulation (Fig. S4a,b) and the strength of the modulation  $\delta J$  (Fig. S4c,d). Given the underlying structure of the materials, we consider a harmonic profile with  $C_6$  symmetry taking the form

$$J(\mathbf{r}) = c_0 + c_1 \sum_{\mathbf{G}} \cos \mathbf{G} \cdot \mathbf{r} \quad (3)$$

where  $\mathbf{G}$  are the reciprocal lattice vectors of the triangular lattice moiré unit cell. We take by definition

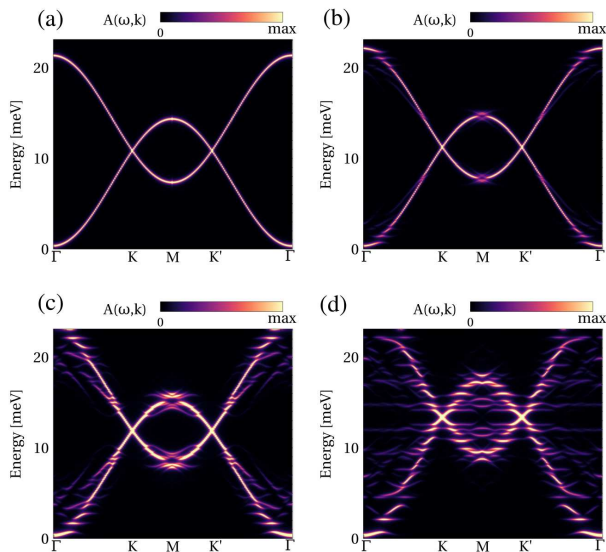


FIG. S5. (a-d) Magnon spectral function unfolded to the minimal unit cell, for strength modulation  $\delta J = 0$  (a)  $\delta J = 0.3\langle J \rangle$  (b),  $\delta J = 0.6\langle J \rangle$  (c),  $\delta J = 1.2\langle J \rangle$  (d).

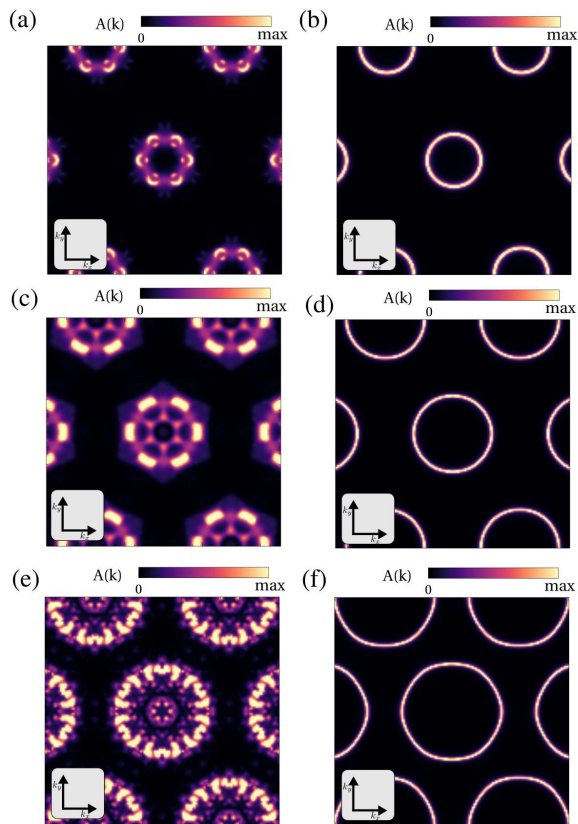


FIG. S6. Unfolded magnon spectral function at a fixed energy with (a,c,e) and without (b,d,f) the moiré exchange modulation. In the presence of the moiré, the emergence of features close to the  $\Gamma$  point is observed in the whole energy range.

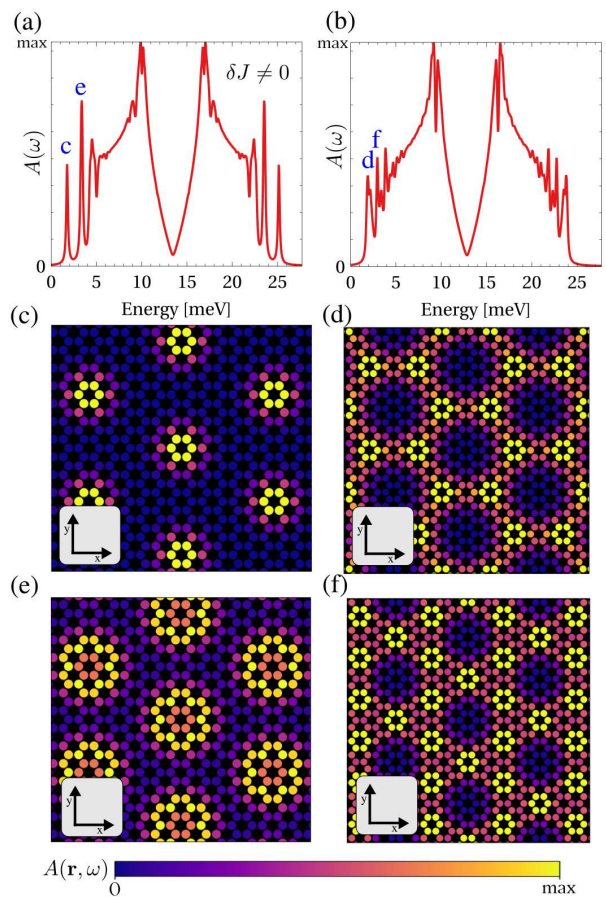


FIG. S7. (a,b) Magnon spectral function and (c-f) real-space distribution of the modes marked in panels (a,b). It is observed that the moiré singularities lead to moiré modes showing a non-uniform distribution in the moiré unit cell.

$\langle J \rangle = \langle J(\mathbf{r}) \rangle$ , and  $\delta J = \max[J(\mathbf{r})] - \min[J(\mathbf{r})]$ , and we consider the two distributions shown in Fig. S4e,f. Panels Fig. S4a,c correspond to the profile Fig. S4e (minimum at  $\mathbf{r} = 0$ ), and panels Fig. S4b,d correspond to the profile Fig. S4f (maximum at  $\mathbf{r} = 0$ ). It is observed that in both cases moiré magnon bands appear at low energies, and with an energy splitting decreasing as the moiré length gets bigger (Fig. S4a,b). The splitting between low energy modes increases as the  $\delta J$  modulation becomes stronger, as shown in (Fig. S4c,d).

The appearance of moiré magnons can also be observed in the unfolded magnon structure, as shown in Fig. S5. In particular, the evolution of the magnon spectral function with increasing modulation strength shows the appearance of moiré mini-bands, which are ultimately responsible of the inelastic quasiparticle interference observed experimentally. This can be observed by computing the isosurfaces of the magnon moiré modes, unfolded to the original moiré unit cell as shown in Fig. S6a,c,e. In particular, it is clearly observed the emergence of short wavelength features in the whole energy range when moiré is switched on. In start contrast, in the absence of



a moiré pattern (Fig. S6b,d,f) the isosurfaces are featureless. Finally, associated with the magnon reconstruction, the spatial distribution is expected to be affected. In Fig. S7, we show the moiré magnon spectra for a specific moiré strength, for the two profiles shown in Fig. S4e,f. It is observed that the low energy moiré magnons show a non-uniform distribution in the moiré unit cell (Fig. S7c-f), featuring emergent triangular, honeycomb and Kagome magnon lattices.

## S5. DRIFT CORRECTION AND SYMMETRIZATION OF RAW IMAGES

The signal to noise ratio of the raw QPI images are enhanced in two steps. At first, the raw constant current topography and  $dI/dV$  maps are corrected for both piezoelectric mechanical creep and thermal drift by algorithm developed by Lawler-Fujita<sup>14</sup>. Finally the drift corrected fourier transform is symmetrized due to the present  $C_6$  symmetry of the crystal lattice. The raw, drift corrected and symmetrized images are shown in (Fig. S8a-i).

---

\* Email: [somesh.ganguli@aalto.fi](mailto:somesh.ganguli@aalto.fi), [jose.lado@aalto.fi](mailto:jose.lado@aalto.fi), [peter.liljeroth@aalto.fi](mailto:peter.liljeroth@aalto.fi)

- <sup>1</sup> Guohong Li and Eva Y. Andrei, "Observation of Landau levels of Dirac fermions in graphite," *Nat. Phys.* **3**, 623–627 (2007).
- <sup>2</sup> T. Matsui, H. Kambara, Y. Niimi, K. Tagami, M. Tsukada, and Hiroshi Fukuyama, "STS observations of Landau levels at graphite surfaces," *Phys. Rev. Lett.* **94**, 226403 (2005).
- <sup>3</sup> Changsong Xu, Junsheng Feng, Hongjun Xiang, and Laurent Bellaiche, "Interplay between Kitaev interaction and single ion anisotropy in ferromagnetic  $\text{CrI}_3$  and  $\text{CrGeTe}_3$  monolayers," *npj Comput. Mater.* **4**, 57 (2018).
- <sup>4</sup> Alexey Kartsev, Mathias Augustin, Richard F. L. Evans, Kostya S. Novoselov, and Elton J. G. Santos, "Biquadratic exchange interactions in two-dimensional magnets," *npj Comput. Mater.* **6**, 150 (2020).
- <sup>5</sup> Lebing Chen, Jae-Ho Chung, Bin Gao, Tong Chen, Matthew B. Stone, Alexander I. Kolesnikov, Qingzhen Huang, and Pengcheng Dai, "Topological spin excitations in honeycomb ferromagnet  $\text{CrI}_3$ ," *Phys. Rev. X* **8**, 041028 (2018).
- <sup>6</sup> Xiaobo Lu, Ruixiang Fei, Linghan Zhu, and Li Yang, "Meron-like topological spin defects in monolayer  $\text{CrCl}_3$ ," *Nat. Commun.* **11**, 4724 (2020).
- <sup>7</sup> D. Soriano, C. Cardoso, and J. Fernández-Rossier, "Interplay between interlayer exchange and stacking in  $\text{CrI}_3$  bilayers," *Solid State Commun.* **299**, 113662 (2019).
- <sup>8</sup> Nikhil Sivadas, Satoshi Okamoto, Xiaodong Xu, Craig J. Fennie, and Di Xiao, "Stacking-dependent magnetism in bilayer  $\text{CrI}_3$ ," *Nano Lett.* **18**, 7658–7664 (2018).
- <sup>9</sup> Weijong Chen, Zeyuan Sun, Zhongjie Wang, Lehua Gu, Xiaodong Xu, Shiwei Wu, and Chunlei Gao, "Direct observation of van der Waals stacking-dependent interlayer magnetism," *Science* **366**, 983–987 (2019).
- <sup>10</sup> Tiancheng Song, Qi-Chao Sun, Eric Anderson, Chong Wang, Jimin Qian, Takashi Taniguchi, Kenji Watanabe, Michael A. McGuire, Rainer Stöhr, Di Xiao, Ting Cao, Jörg Wrachtrup, and Xiaodong Xu, "Direct visualization of magnetic domains and moiré magnetism in twisted 2d magnets," *Science* **374**, 1140–1144 (2021).
- <sup>11</sup> T. Holstein and H. Primakoff, "Field dependence of the intrinsic domain magnetization of a ferromagnet," *Phys. Rev.* **58**, 1098–1113 (1940).
- <sup>12</sup> D. Ghazaryan, M. T. Greenaway, Z. Wang, V. H. Guarochico-Moreira, I. J. Vera-Marun, J. Yin, Y. Liao, S. V. Morozov, O. Kristanovski, A. I. Lichtenstein, and et al., "Magnon-assisted tunnelling in van der Waals heterostructures based on  $\text{CrBr}_3$ ," *Nat. Electron.* **1**, 344–349 (2018).
- <sup>13</sup> Wei-Bing Zhang, Qian Qu, Peng Zhu, and Chi-Hang Lam, "Robust intrinsic ferromagnetism and half semiconductivity in stable two-dimensional single-layer chromium trihalides," *J. Mater. Chem. C* **3**, 12457–12468 (2015).
- <sup>14</sup> MJ Lawler, K Fujita, Jhinwan Lee, AR Schmidt, Y Kohsaka, Chung Koo Kim, H Eisaki, S Uchida, JC Davis, JP Sethna, et al., "Intra-unit-cell electronic nematicity of the high- $T_c$  copper-oxide pseudogap states," *Nature* **466**, 347–351 (2010).

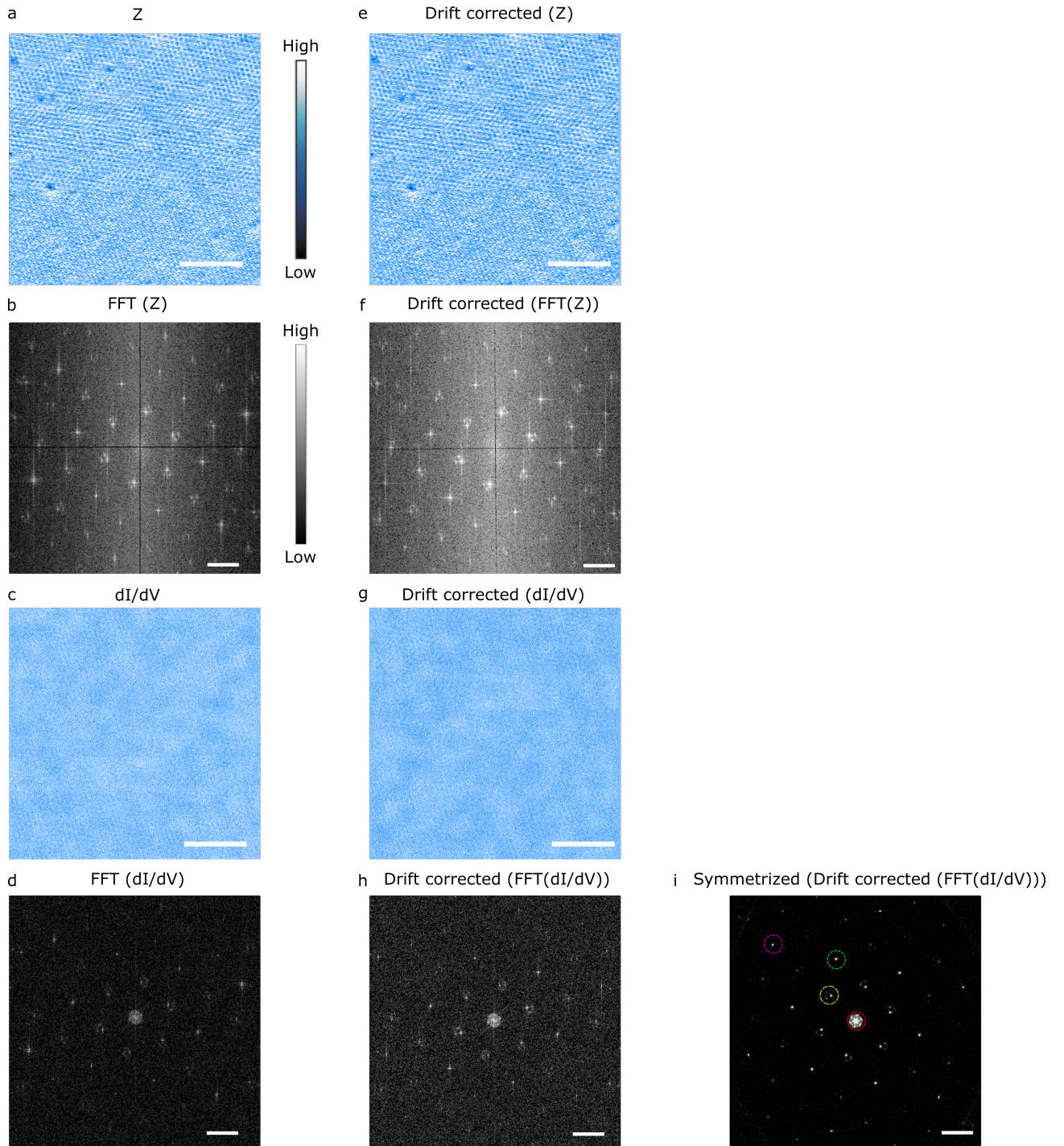


FIG. S8. Real space images and fourier transforms after each step: (a),(b) Raw topographic image and its fast fourier transform (FFT), (c), (d) raw tunneling conductance ( $dI/dV$ ) and its FFT. Drift corrected (Lawler-Fujita algorithm) (e), (f) topographic image and its FFT, (g), (h) ( $dI/dV$ ) and its FFT. (i) 3-fold symmetrised FFT. Constant current map taken at bias  $V= 2.3$  mV, r.m.s modulation= $120 \mu V$  setpoint= 200 pA. The scale bars for real space images (a,c,e,g) 15 nm. The scale bars for reciprocal space images (b, d, f, h, i) are  $5 \text{ nm}^{-1}$ . In (i) red, yellow, green and magenta dotted circles indicate real space length scales of 7 nm, 1.25 nm, 6 Å, 4 Å respectively.